Observation of force-detected nuclear magnetic resonance in a homogeneous field

L. A. Madsen, G. M. Leskowitz, and D. P. Weitekamp*

Arthur Amos Noyes Laboratory of Chemical Physics, California Institute of Technology, MC 127-72, Pasadena, CA 91125

Communicated by John D. Roberts, California Institute of Technology, Pasadena, CA, July 19, 2004 (received for review May 29, 2003)

We report the experimental realization of BOOMERANG (better observation of magnetization, enhanced resolution, and no gradient), a sensitive and general method of magnetic resonance. The prototype millimeter-scale NMR spectrometer shows signal and noise levels in agreement with the design principles. We present ^{1}H and ^{19}F NMR in both solid and liquid samples, including time-domain Fourier transform NMR spectroscopy, multiple-pulse echoes, and heteronuclear *J* spectroscopy. By measuring a ^{1}H-^{19}F *J* coupling, this last experiment accomplishes chemically specific spectroscopy with force-detected NMR. In BOOMERANG, an assembly of permanent magnets provides a homogeneous field throughout the sample, while a harmonically suspended part of the assembly, a detector, is mechanically driven by spin-dependent forces. By placing the sample in a homogeneous field, signal dephasing by diffusion in a field gradient is made negligible, enabling application to liquids, in contrast to other force-detection methods. The design appears readily scalable to μm-scale samples where it should have sensitivity advantages over inductive detection with microcoils and where it holds great promise for application of magnetic resonance in biology, chemistry, physics, and surface science. We briefly discuss extensions of the BOOMERANG method to the μm and nm scales.

Today, multiple-pulse Fourier transform NMR (FTNMR) is a nondestructive method of spectroscopy and imaging in solutions and solids with exquisite chemical specificity and information content. The power of NMR as an analytical tool in studies of molecular structure determination and dynamics is largely caused by its coherent nature, which allows tremendous finesse in selectively enhancing or suppressing interactions in a system of interest.

Although the detection method for most of the development of NMR has been the Faraday law induction method of Purcell *et al*. (1) and Bloch *et al*. (2), the first method of NMR was a gradient-based method of force detection, the molecular beam deflection method of Rabi *et al*. (3). The detection of NMR by observing the change in force on a sample in a field gradient upon saturation of the spins was introduced by Evans (4). Sidles and collaborators (5–7) introduced cyclic modulation of this force at the frequency of a mechanical resonator bearing the sample or a nearby magnet in the method of magnetic resonance force microscopy (MRFM), which allows force detection of magnetic resonance imaging of solid samples and has favorable prospects for scaling to smaller samples with inversely proportional larger gradients. A mechanical detection method suitable for condensed phase samples in homogeneous fields was introduced by Gozzini and coworkers (8, 9), who measured the torque on a suspended sample caused by the transfer of angular momentum by spin-lattice relaxation of electron spins.

Recently, we proposed a method of force-detected magnetic resonance (10) that eliminates the field gradient across the sample, while simultaneously optimizing the signal-to-noise ratio (SNR) for spin-dependent forces or torques. The goal is better observation of magnetization, enhanced resolution, and no gradient (BOOMERANG) relative to both inductive detection and other mechanical methods of magnetic resonance. Like inductive detection, BOOMERANG uses a homogeneous magnetic field and so is general with respect to pulse sequence, the geometry and thermodynamic phase of the sample, and whether a field gradient is introduced to encode magnetic resonance imaging information. As in MRFM, the sensitivity of BOOMERANG scales more favorably than inductive detection for small samples and detectors. The key goal is higher-sensitivity NMR for small samples, including surfaces. Shrinking the sample volume necessary for NMR will facilitate analysis of large-sample libraries. Additionally, reducing the size of the hardware lowers the mass and power consumption, important considerations for remote sensing and other portable applications.

Fig. 1 depicts the prototype BOOMERANG spectrometer. The ferromagnetic assembly entails two pole pieces with diameter substantially larger than that of the sample. In the center of each pole piece a cylindrical detector magnet, comparable in diameter to the sample, has been placed in a closely fitting orifice. The sample exerts a force on the detector magnet that is proportional to the *z*-component of the sample's magnetization. One may think of the interaction between the sample and detector magnet dipoles as equivalent to the force between axially aligned bar magnets, but this force is achieved in a geometry that places no field gradient across the sample. This can be described (10) as an "inverse Stern-Gerlach force," the inner product of the gradient of the sample's field and the ferromagnetic dipole of the detector. This detector magnet is fixed to a flexible silicon beam and this composite mechanical resonator exhibits a high-quality harmonic motion along the *z* axis. The sample's spin magnetization is inverted twice per resonator period by radio frequency (rf) pulses at the Larmor frequency supplied by the coil inductor, resulting in a force on the resonator at its fundamental frequency. The resulting spin-driven motion of the resonator is the signal and is detectable by a displacement sensor, such as those used in atomic force microscopy. To minimize disturbance to the field homogeneity, this motion could be measured and compensated in a feedback loop, but here it is small enough ($<$1 nm) to have negligible effect on the spins.

For NMR, we keep the sample stationary and use cyclic adiabatic rapid passage (ARP) of the rf through the Larmor frequency of the spins to drive the mechanical resonator with an amplitude (including sign) proportional to the longitudinal spin magnetization M_z of the sample. To encode an NMR experiment into the observable M_z, this ARP detection period is preceded by a period of spin evolution, which is typically incremented on successive repetitions of the experiment. This encoding period may include any of the rf pulse sequences used in multiple-pulse and multidimensional NMR, maximizing the types of spectroscopic information available.

Fig. 2 depicts a simple case, the measurement of a free evolution transient and its FTNMR spectrum by using BOOMERANG. During t_1, transverse magnetization created by

Abbreviations: BOOMERANG, better observation of magnetization, enhanced resolution, and no gradient; FTNMR, Fourier transform NMR; MRFM, magnetic resonance force microscopy; SNR, signal-to-noise ratio; rf, radio frequency; ARP, adiabatic rapid passage.

*To whom correspondence should be addressed. E-mail: weitekamp@caltech.edu.

© 2004 by The National Academy of Sciences of the USA

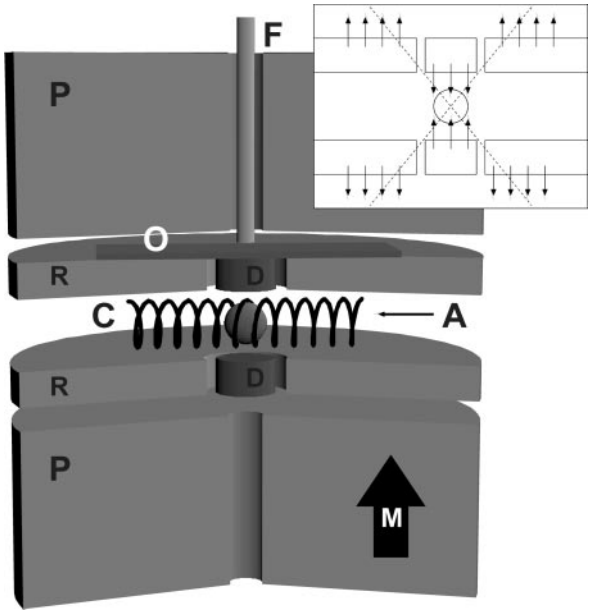

Fig. 1. Cutaway diagram of the BOOMERANG spectrometer. Two NdFeB pole magnets P magnetize a cylindrically symmetric array formed by ring magnets R and detector magnets D, which are made of mu-metal. A spherical volume A, filled with a liquid or solid sample, is placed inside coil C, which provides rf pulses to modulate the sample's magnetization. The magnet assembly, which may be viewed as a pair of pole pieces slightly perturbed by removal of the material to form the gap around the detector magnets D, provides a homogeneous field of ≈0.65 T at the sample. One of the detector magnets is fixed to a single-crystal silicon beam O forming a *z*-axis mechanical resonator with fundamental frequency ≈450 Hz. (*Inset*) This cross section shows the forces exerted by the sample on the components of the magnet array when the magnetizations of the sample and all of the magnets are aligned along vector M. Cyclic inversion of the sample's magnetization induces mechanical oscillations of O, which are detected with fiber-optic interferometer F. Also shown is a cone-shaped nodal surface where the axial component of the magnetic force vanishes. The cylindrical detector magnet D is contained within this cone and it is roughly the same volume as the spherical sample volume for which the detector geometry is optimized (10).

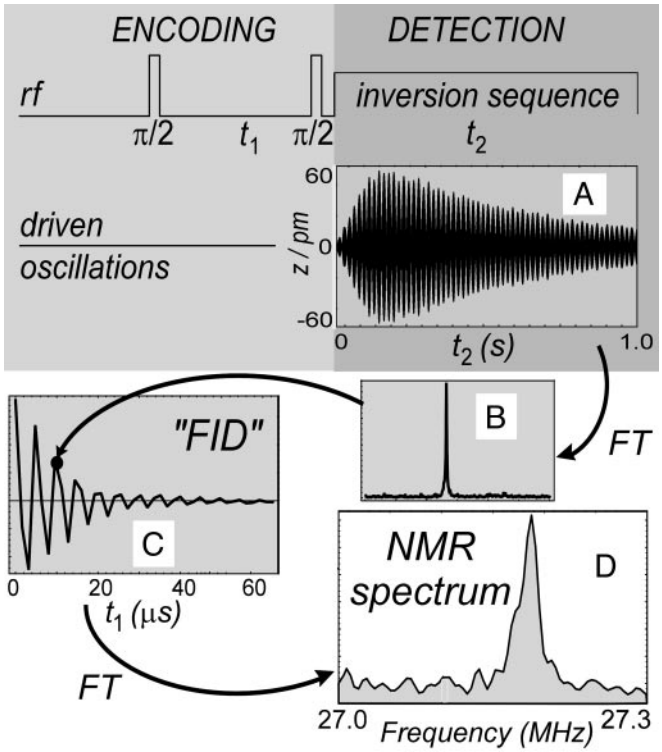

Fig. 2. NMR spectroscopy with BOOMERANG. The resonator is driven by cyclic inversion of the sample's magnetization, and a mechanical displacement signal A is recorded during the detection period t_2 for a given value of the evolution period t_1. The Fourier transform (FT) of *A* yields a spectrum *B* with a peak at the mechanical resonator frequency. The area (and height) of this peak is proportional to the spin magnetization M_z present at the start of the detection period. Weighting of the spectrum (*B*) gives a single point in the NMR time-domain signal (*C*). The NMR pulse sequence in the encoding period is used to modulate M_z as a function of t_1 to build up this signal point by point. The Fourier transform of the signal vs. t_1 gives the 1D FTNMR spectrum (*D*). All data were collected on protons in a 2.6-mm sphere of water by using our prototype BOOMERANG spectrometer without averaging, where the total acquisition time was 8 min (40 points in t_1 at 12-s intervals).

the first pulse evolves under the total spin Hamiltonian, which includes both the interaction of the spins with the static field and any spin–spin interactions. This transverse magnetization, at any given time after the first pulse, is the same as would be observed as a free induction decay in inductive NMR. After the time t_1, the second $\pi/2$ pulse converts one component of the transverse magnetization (M_x or M_y) to longitudinal magnetization M_z, which is measured in the detection period t_2 by driving the mechanical resonator by using cyclic spin inversion. The amplitude and sign of the oscillation at the driving frequency is extracted by Fourier transformation with respect to t_2 or by matched filtering. This amplitude becomes one point in the time-domain NMR signal that results from repeating the pulse sequence for incremental values of t_1. Fourier transformation with respect to t_1 yields the NMR spectrum. All data depicted in Fig. 2 were collected on liquid water and represent an observation of NMR on a fluid by using force detection. The observed amplitude of mechanical resonator displacement shown in Fig. 2 *A* and *B* is midway between the value expected for sinusoidal modulation of M_z (10) and the value (27% greater) that would be seen in the limit of square wave modulation. This agreement with theory is within the uncertainties (≈20%) primarily caused by imprecision in the knowledge of the sample position and volume.

The linewidth of the FTNMR spectrum in Fig. 2*D* is 8 kHz (≈300 ppm), an inhomogeneous broadening predominantly caused by imperfect manufacture and alignment of the detector and annular magnets. Finite element simulations indicate that with ideal placement of magnetic material, an annular gap 1/40 of the detector magnetic diameter allows for a homogeneous linewidth of 1 ppm (MAXWELL software, Ansoft, Pittsburgh), so improvement is possible with this geometry. An alternative approach to the high resolution desirable for chemical-shift studies would be to perform the NMR evolution period in a region without sample-scale magnet features, where field homogeneity is achievable with less stringent machining tolerances. Shuttling the sample between such an evolution region and the detector region is compatible with the timeline of Fig. 2, since the longitudinal magnetization can be stored for times short, compared with T_1, while the sample is in motion. By shuttling the sample to a distance 10 radii away from the detection region, the inhomogeneity caused by the gap around the sensor is decreased by another 2 orders of magnitude, making it irrelevant to the achievable spectral resolution. Such a shuttling capability could be incorporated into an automated sample transport system that is a desirable feature for many submillimeter-scale applications of NMR. Because the rf circuit used for the evolution period plays no direct role in the sensitivity, it should be possible to separately optimize homogeneity, spin excitation, and detector sensitivity, thereby eliminating tradeoffs that reduce performance in all of these factors.

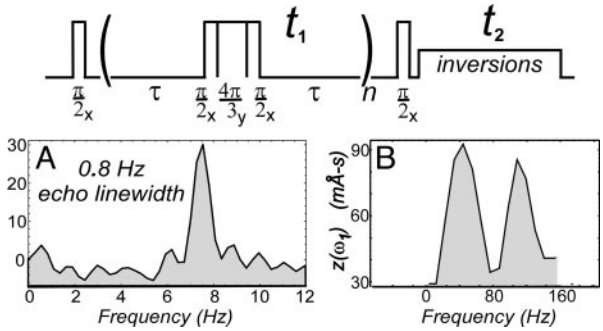

Fig. 3. Spin echo and *J* spectroscopy. The encoding period of Fig. 2 is modified to include composite inversion pulses to refocus residual magnetic field inhomogeneity. (*A*) Spin-echo spectrum of water. (*B*) Measurement of the fluorine-hydrogen *J* coupling in a fluoroacetonitrile sample (CH_2FCN). The echo-period pulse sequence (*Upper*) was applied with inversion pulses at both the ^1H and ^{19}F Larmor frequencies followed by proton detection. The delay $\tau =$ 240 μs and the length of a $\pi/2$ pulse was 3.6 μs. Both spectra are shown referenced to the 29-MHz carrier (NMR pulse) frequency.

The observed inhomogeneous linewidth of Fig. 2 is already 3,000 times narrower than would be observed without the compensating magnets that embody the BOOMERANG concept. One consequence is that the sample volume contributing to the signal (the entire sphere) is ≈100 times greater than that of a sensitive slice through the spherical sample that would be practical with the optimized detector magnet alone, as in the case of MRFM. The paramount advantage of BOOMERANG detection lies in providing field homogeneity sufficient for prolonged coherent spin manipulations and inversions of the entire sample magnetization. This process allows optimal application of the full scope of modern time-domain NMR spectroscopy and imaging pulse sequences. Coherent control over the entire sample volume is important not only in the detection period, but even more so in the evolution period if multiple-pulse experiments for line narrowing and other purposes are to be effective. These can provide spectral narrowing of terms in the spin Hamiltonian by several orders of magnitude but typically require the inhomogeneous spectral width to be <100 kHz to allow coherent control with practical excitation bandwidths (typically comparable to the Rabi frequency).

For samples with translational diffusion, as in liquid samples, there is another important motivation for achieving this degree of homogeneity. Since diffusion of spin-bearing molecules through field gradients becomes a dominant mechanism of irreversible dephasing in a substantially inhomogeneous field, BOOMERANG is essential to sensitive force detection of liquids and other diffusing phases. Since this gradient-induced irreversible dephasing scales with $(dB_z/dq)^2$, where q is the coordinate in the gradient direction (10–12), the reduction in inhomogeneity observed with the prototype translates into a factor of 10^7 reduction in this dephasing rate, enabling force-detected NMR of a fluid. This dephasing mechanism limits high-sensitivity MRFM (7) to investigation of solid or frozen samples.

With such diffusion-induced dephasing mitigated by eliminating the gradient, a variety of spin-echo experiments are possible, which extends the capability of spectrometers with modest field homogeneity. In particular, trains of π (echo) pulses both eliminate static in homogeneity and further reduce dephasing caused by diffusion in residual gradients (11). Fig. 3 illustrates the echo capabilities of the BOOMERANG prototype for homonuclear and heteronuclear spin echoes. A composite π pulse (13), illustrated at the top of Fig. 3, was used to invert the entire magnetization over the inhomogeneous linewidth. Using a water sample, we obtained a linewidth of <1 Hz (Fig. 3*A*) by Fourier transformation of the echo amplitude as a function of t_1. The heteronuclear *J* spectrum obtained on a 2.6-mm sphere of fluoroacetonitrile (CH_2FCN) uses the pulse sequence of Fig. 3 with echo pulses at both the fluorine and proton frequencies to observe the *J* coupling between the fluorine and protons as a doublet splitting of the proton echo spectrum.

Before conducting pulsed FTNMR experiments, we optimized experimental parameters by measuring the sample's T_1 by inversion recovery and by characterizing the rf field (B_1) strength by performing nutation. Our inversion-recovery pulse sequence is (π-t_1-DETECT), where the t_1 time variable is incremented on successive repetitions of the experiment. We have recorded the ^1H T_1 as 4.3 s in liquid water and 7 s in solid ammonium nitrate. For ^{19}F in fluoroacetonitrile, $T_1 = 1.7$ s. The nutation sequence is (θ-DETECT), where the pulse angle θ is the incremented variable. The 90° pulse time is adjustable down to 1.8 μs by using an untuned rf coil.

Elsewhere (10) we have discussed, for sample radii r in the range of a few microns to a few millimeters, the theoretical expectations for the SNR of BOOMERANG and inductive detection as the detector and sample are scaled down together. Specifically, we compared the optimal BOOMERANG approach to the most sensitive implementation of inductively detected NMR in which ideal spin-locking during detection (14) was hypothetically achieved. This comparison results in the respective SNR expressions for a single repetition

$$SNR_B = \frac{\kappa_F \mu_0 V_s M_s M_d / R_{max}}{\sqrt{16 k_B T m / \tau_h T_{1a}}} \quad [1]$$

$$SNR_I = \frac{\kappa_I \mu_0 V_s M_s \omega_0 / R_{max}}{\sqrt{8 k_B T R / T_{1\rho}}}. \quad [2]$$

Here V_s is the volume of the sample, M_s is the magnetization of the sample at $t_2 = 0$, M_d is the magnetization of the detector magnet, R_{max} is the distance of closest approach of the detector (magnet or inductive coil) to the sample center, T is the temperature of the detector, ω_0 is the Larmor frequency, k_B is Boltzmann's constant, μ_0 is the permeability of free space, and R is the resistance of the inductive coil. The dissipation of the mechanical resonator is completely determined by its ringdown time τ_h and its motional mass m. The times T_{1a} and $T_{1\rho}$ describe the decay of the magnetization during the ARP driving and spin-locking, respectively, that limits the duration of each acquisition and thus determines the noise bandwidth. The coefficients κ_F and κ_I are obtained by numerical integrations (10) that relate to the geometries of the sample and the detector magnet or inductive coil, respectively. To maximize force sensitivity, the interaction force between the detector magnet and the sample must be balanced against the motional mass of the mechanical resonator. The aspect ratio and shape of the magnet, along with the motional mass of the resonator suspension, influence the optimum detector magnet geometry. For a spherical sample volume, constraining the detector magnet shape to be a right cylinder allows for ease of design and manufacture and simplified optimization of field homogeneity, while sacrificing less than a factor of 1.4 in force sensitivity relative to an arbitrary solid of revolution about z (15). To minimize acoustic and viscous losses and coupling to external acoustic noise, the mechanical resonator should operate in vacuum. In the prototype, the entire magnet assembly operates at ≈10 mTorr inside a bell jar. The picometer vibrations induced in the resonator by the force of the sample magnetization are measured by fiber optic interferometry (16). We measured a displacement noise amplitude of 0.7 pm/(Hz)$^{1/2}$ at the mechanical resonator frequency. This noise was dominated by the Brownian motion noise amplitude of 0.5

pm/(Hz)$^{1/2}$ calculated by using the measured resonator frequency, temperature, and ringdown time and measured from the magnitude spectrum with no resonator driving. The excess noise is white in the vicinity of the mechanical resonance and is apparently dominated by laser intensity noise in the fiber optic interferometer. This excess noise will become even less important fractionally for smaller versions of the apparatus.

This apparatus is also potentially valuable for measuring static magnetic moments. Since magnetic field at the sample is often an important state variable, a homogeneous field across the sample is a desirable feature for magnetic susceptometry and magnetic resonance. Notably, at room temperature the prototype's sensitivity to magnetic moments of 1×10^{-11} EMU/(Hz)$^{1/2}$ is 50 times better than that of a millimeter-scale commercial high field SQUID magnetometer operating at 4 K (17). Magnetic susceptometry may be implemented by cyclically moving the sample at half the resonator frequency around the position of maximum coupling, thus resonantly driving the detector with the static moment of the sample.

The prototype mechanical resonator consists of a $23.0 \times 2.6 \times 0.22$-mm single-crystal silicon beam soldered to both the cylindrical detector magnet, 3 mm in diameter by 1.5 mm in height, and to the annular magnet, both machined from HyMu80 (Carpenter Specialty Alloys, Wyomissing, PA). Resonators typically resonate at 450 Hz with a ring-down time of 85 ms. Samples are held in spherical bulbs within a nine-turn, 4-mm diameter solenoid rf coil. The static magnetic field of 0.63–0.69 T is generated by a pair of cylindrical, axially polarized NdFeB magnets 50 mm in diameter by 25 mm thick. Rf pulses and cyclic inversion sequences are generated in the range 1 to 5 MHz by an arbitrary waveform generator (AWG502, Signatec, Corona, CA) and mixed up to NMR frequencies via a single-sideband mixer. The untuned rf coil allows for simultaneous excitation pulses on protons and other nuclei. Fiber-optic interferometer signals are amplified, bandwidth-limited, and digitized directly at greater than twice the mechanical resonator frequency before Fourier transformation to obtain the mechanical frequency spectrum.

Frequency shifts of the mechanical resonator during rf irradiation were initially a problem. This problem was mitigated by enclosing the rf excitation coil in a Faraday cage consisting of a brass sheet 25 μm thick. This finding suggests that the rf was heating the resonator components. Using this shield, we have conducted experiments with signal averaging of up to 3 h with minimal resonator frequency drift while using no active feedback on the temperature or the resonator motion. Phase fluctuations of several degrees in the spin-driven resonator response were observed and dominated the noise for the largest signals. This is a form of multiplicative t_1 noise (14) and suggests that further stabilization is needed to approach the Brownian sensitivity limit over the full dynamic range of the NMR signals.

Cyclic inversion of the longitudinal magnetization in the detection period t_2 was achieved by ARP with digitally generated frequency sweeps through resonance. It was observed that when the frequency was swept back and forth through resonance in each mechanical period T, a spin-independent driving of the resonator was observed. This background driving was eliminated by performing all frequency sweeps in the same direction (e.g., low to high in frequency), leaving only the desired spin-dependent driving.

The observed decay time T_{1a}' of the longitudinal magnetization M_z during resonator driving ideally approaches the intrinsic spin relaxation time T_{1a} characteristic of the sample under ideal cyclic inversion. This ideal time is bounded by the spin-lattice relaxation time T_1 and the spin-locked relaxation time $T_{1\rho}$, which are nearly equal for molecules tumbling isotropically at rates in excess of the Larmor frequency. In initial experiments using a tangent-modulated (18) frequency sweep designed for adiabatic inversion over a range of resonance offsets and rf field strengths,

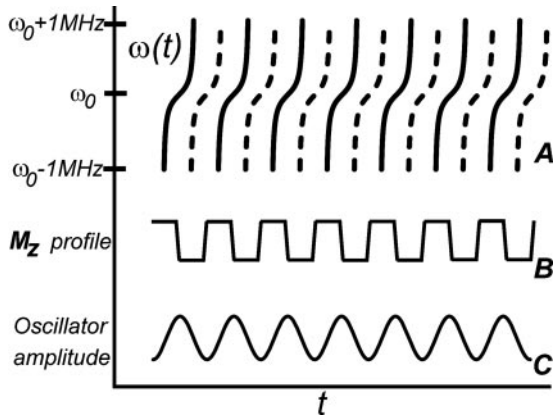

Fig. 4. Phase-cycled, tangent-modulated ARP detection sequence. (*A*) Rf modulation through the NMR line during ARP. The rf phase alternates between 0 and π on successive ARP sweeps, as indicated by alternating dashed and solid lines. The sign of the frequency sweep is identical for all inversions, which places the predominant Fourier component of the rf modulation at twice the resonator frequency and thus reduces spurious resonator driving by the rf. (*B*) Time dependence of the z-magnetization M_z induced in the sample by the cyclic inversion sequence. (*C*) The spin-driven mechanical resonator amplitude lags M_z by $\pi/2$ in phase.

we observed $T_{1a}' \ll T_1$, suggesting an unanticipated nonadiabaticity. This extra decay was largely corrected by introducing an rf phase shift of π between successive sweeps through resonance. Fig. 4 depicts our ARP excitation scheme and the corresponding magnetization and resonator responses. For both liquid and solid samples, this phase-shifted sequence increased T_{1a}' by up to 4-fold and brought it within a factor of 2 of T_1. Since SNR scales as $(T_{1a}')^{-1/2}$, an experimental transient with $T_{1a}'/T_{1a} = 0.5$ is within 70% of being optimal with respect to spin inversion. If we model the excess decay as caused by a spin inversion efficiency per pulse of $f_e < 1$, then $T_{1a}' = T_{1a}T/(T - 2T_{1a}\ln f_e)$. With $T =$ 2 ms, obtaining $T_{1a}'/T_{1a} = 0.5$ corresponds to $f_e = 0.999$ (99.9% inversion efficiency), so indeed these experiments exhibit nearly perfect adiabatic spin inversion.

Any modern NMR experiment can be adapted to longitudinal force detection with BOOMERANG by simply inserting the desired pulse sequence into the encoding period of the pointwise acquisition protocol shown in Fig. 2. In contrast to MRFM, which is restricted to imaging methods based on sensitive slices normal to the gradient direction (5, 6), BOOMERANG should enable the use of modern imaging protocols that rely on homogeneous fields and switchable DC or rf gradients to encode multiple pixels into the observed volume, which can be the whole 3D sample or a 2D slice at any orientation. For use with BOOMERANG detection, these pulsed gradients could be introduced in the encoding periods with suitable coils or with controlled displacements of the BOOMERANG magnets (19).

When a scale invariant mechanism of mechanical damping dominates, the BOOMERANG SNR is proportional to $r^{1/2}$, where r is the sample radius and other dimensions are assumed to scale identically. Eddy current damping is such a mechanism and dominates in the prototype. Raising the resistivity of the ferromagnetic material on and near the resonator and interrupting the paths of eddy currents with insulating barriers are strategies for further increasing the ringdown time. The SNR of inductive detection scales as r^2 in this range of sizes and the sensitivity curves for the two methods cross at r values, typically in the 10- to 1,000-μm range, that depend on the field strength and gyromagnetic ratio (10), with BOOMERANG having its greatest predicted advantages at low Larmor frequencies.

This finding suggests such applications as portable NMR and massively parallel NMR, where the high mass and/or cost of superconducting magnets preclude their use. The weak scaling of BOOMERANG sensitivity with length scale favors massive parallelism with smaller detectors, unlike inductive detection. For instance, suppose that a given sample volume is subdivided to be analyzed by an array of 10^4 detectors, each with length scale smaller by $10^{4/3}$ than the single device needed to measure the whole sample in one detector. If SNR scales as $r^{1/2}$, then averaging the results from the array gives a sensitivity advantage of $((10^4)^{1/2})/((10^{4/3})^{1/2}) = 10^{4/3} = 21.5$ over the single-detector measuring the entire sample. If instead SNR scales as r^2, the array is less sensitive by $((10^4)^{1/2})/((10^{4/3})^2) = 10^{-2/3} = 0.215$. Thus BOOMERANG is favorable for signal averaging not only in time, as in traditional spectroscopy, but also in space.

Even more favorable scaling of SNR applies if instrument noise is sufficiently low to allow measurement of fluctuations in the spin magnetization, which exceed the mean signal for small polarization and number of spins. In this regime, BOOMERANG is predicted to enable the CONQUEST measurement paradigm (correlated observations narrow quantum uncertainty, enhancing spectroscopic transients) (15, 20, 21), which uses measurements made before and after the spin evolution period to encode coherent NMR on the spin magnetization fluctuations.

In BOOMERANG, the aligned dipoles in the ferromagnetic annular and detector magnets create a negative contribution to the spring constant for the resonator's motion along the z axis, softening the mechanical mode. This process allows use of short beams, which are both light (minimizing the motional mass) and robust (facilitating manufacture without breakage). In our prototype, we have observed reductions in resonance frequency upon application of a magnetic field by factors of 1.4–2.5 depending on the value of the elastic force constant [ranging from 7,000 to 10,000 N/m with different silicon beams (21)] relative to the magnetic force constant, which is deduced to be $-6{,}000$ N/m for our magnet geometry and field strength of $\approx$0.65 T. The use of magnetic forces in the suspension of the detector is key to scaling down the motional mass along with the sample volume. With all dimensions scaled identically, the scaling for mechanical frequency is generally r^{-1}, limiting the size range over which audio frequency resonators can be implemented, as is necessary to couple to practical rates of cyclic inversion. For BOOMERANG this range will be extended because of the mechanical frequency reduction afforded by the magnet assembly design. A lowered mechanical resonance frequency at a given beam size is also expected to reduce some contributions to the damping rate, such as thermoelastic damping (22). We have described progress (23) toward a micromachined BOOMERANG, with a 50-μm diameter detector magnet and 1-μm annular gap, fabricated with photolithography, deep reactive-ion etching, and electrodeposition.

Coupling a mechanical motion near the Larmor frequency to the transverse magnetization is another strategy for scaling down force detection (24). This appears to be necessary for reaching the nanoscale without sacrificing sensitivity, as would occur if the motional mass were kept larger than r^3 scaling would suggest. For example, the BOOMERANG geometry of Fig. 1 could be adapted to detecting transverse magnetization by mounting the detector magnet to instead oscillate torsionally around an axis perpendicular to the magnetic field. After shape optimization of the cylinder (15), the SNR and scaling relationships for such designs are similar to the optimum design (10) for the present longitudinal detection method, if compared at similar resonator ringdown times and magnetization decay times, as would be achieved by spin-locking during detection. Thus a mechanism exists whereby the BOOMERANG method could be extended to nanoscale, where practical mechanical motions of optimally sized resonators are in the rf range.

This research was performed for the Center for Space Microelectronics Technology, Jet Propulsion Laboratory, California Institute of Technology, and was sponsored by the National Aeronautics and Space Administration, Office of Space Science.

1. Purcell, E. M., Torrey, H. C. & Pound, R. V. (1946) *Phys. Rev.* **69,** 37–38.
2. Bloch, F., Hansen, W. W. & Packard, M. (1946) *Phys. Rev.* **70,** 474–485.
3. Rabi, I. I., Zacharias, J. R., Millman, S. & Kusch, P. (1938) *Phys. Rev.* **53,** 318.
4. Evans, D. F. (1956) *Philosophical Magazine* **1,** 370–373.
5. Sidles, J. A. (1991) *Appl. Phys. Lett.* **58,** 2854–2856.
6. Yannoni, C. S., Zuger, O., Rugar, D. & Sidles, J. A. (1996) in *Encyclopedia of Nuclear Magnetic Resonance*, eds. Grant, D. M. & Harris, R. K. (Wiley, New York), pp. 2093–2101.
7. Bruland, K. J., Dougherty, W. M., Garbini, J. L., Sidles, J. A. & Chao, S. H. (1998) *Appl. Phys. Lett.* **73,** 3159–3161.
8. Gozzini, A. (1963) in *XII Colloque Ampere*, eds. Servant, R. & Charru, A. (North–Holland, Bordeaux, France), pp. 82–108.
9. Alzetta, G., Arimondo, E., Ascoli, C. & Gozzini, A. (1967) *Il Nuovo Cimento* **52B,** 392–402.
10. Leskowitz, G. M., Madsen, L. A. & Weitekamp, D. P. (1998) *Solid State Nucl. Magn. Reson.* **11,** 73–86.
11. Carr, H. Y. & Purcell, E. M. (1954) *Phys. Rev.* **94,** 630–638.
12. Slichter, C. P. (1990) *Principles of Magnetic Resonance* (Springer, New York).
13. Levitt, M. H. (1986) *Progr. Nuclear Magn. Reson. Spectrosc.* **18,** 61–122.
14. Weitekamp, D. P. (1983) *Adv. Magn. Reson.* **11,** 111–274.
15. Leskowitz, G. M. (2003) Ph.D. thesis (California Institute of Technology, Pasadena).
16. Rugar, D., Mamin, H. J. & Guethner, P. (1989) *Appl. Phys. Lett.* **55,** 2588–2590.
17. Hibbs, A. D., Sager, R. E., Kumar, S., McArthur, J. E., Singsaas, A. L., Jensen, K. G., Steindorf, M. A., Aukerman, T. A. & Schneider, H. M. (1994) *Rev. Sci. Instr.* **65,** 2644–2652.
18. Hardy, C. J. & Edelstein, W. A. (1986) *J. Magn. Reson.* **69,** 196–199.
19. Kempf, J. G. & Marohn, J. A. (2003) *Phys. Rev. Lett.* **90,** 087601.
20. Carson, P. J., Madsen, L. A., Leskowitz, G. M. & Weitekamp, D. P. (2000) U.S. Patents 6,078,872 and 6,081,119.
21. Madsen, L. A. (2002) Ph.D. thesis (California Institute of Technology, Pasadena).
22. Lifshitz, R. & Roukes, M. L. (2000) *Phys. Rev. B* **61,** 5600–5608.
23. George, T., Chang-Chien, A., Madsen, L., Leskowitz, G., Tang, W. & Weitekamp, D. P. (2001) *Aerospace Conf. 2001 IEEE Proc.* **1,** 273–278.
24. Sidles, J. A., Garbini, J. L. & Drobny, G. P. (1992) *Rev. Sci. Instrum.* **63,** 3881–3889.